Co., Cleveland, OH 64th ed., 1983, p F-187.
26. Shannon, R. D.; Prewitt, C. T. *Acta Cryst.* **1969**, *B25*, 925.
27. Jeong, H. K.; Kim, J. S.; No, K. T. The Proceedings of 72nd Annual Meeting of Korean Chemical Society, 1993, p 80.
28. Charnell, J. F. *J. Crystal Growth* **1971**, *8*, 291.
29. Cruz, W. V.; Leung, P. C. W.; Seff, K. *J. Am. Chem. Soc.* **1978**, *100*, 6997.
30. Mellum, M. D., Seff, K. *J. Phys. Chem.* **1984**, *88*, 3560.
31. International Tables for X-ray Crystallography, Kynoch Press, Birmingham, England, 1974, Vol. IV, pp 61-66.
32. Calculations were preformed with *Structure Determination System, MolEN*, Enraf-Nonius, Netherlands, 1990.
33. Blackwell, C. S.; Pluth, J. J.; Smith, J. V. *J. Phys. Chem.* **1985**, *89*, 4420.
34. Doyle, P. A.; Turner, P. S. *Acta Crystallogr., Sect. A*, **1968**, *24*, 390.
35. Reference 31, pp 73.
36. Cromer, D. T. *Acta Crystallogr.* **1965**, *18*, 17.
37. Reference 31, pp 149-150.
38. Yanagida, R. Y.; Amaro, A. A.; Seff, K. *J. Phys. Chem.* **1973**, *77*, 805.
39. Heo, N. H.; Seff, K. *J. Am. Chem. Soc.* **1987**, *109*, 7986.

Theoretical Study of Bonding and Electrical Conductivity in the Ternary Molybdenum Oxide KMo_4O_6

Dae-Bok Kang

Department of Chemistry, Kyungsung University, Pusan 608-736, Korea
Received June 7, 1995

The electronic band structure and electrical properties of KMo_4O_6 containing chains of condensed molybdenum octahedra are analyzed by means of the extended Hückel tight-binding method. KMo_4O_6 has partially filled bands of 1D as well as 3D character. They also exhibit the anisotropic band dispersions with bandwidths much larger along the c^* axis than along the directions perpendicular to it. Thus, conduction electrons are essentially delocalized along the c^* direction (*i.e.*, the chain of condensed molybdenum octahedra) in the solid. The 1D band of two partially filled d-block bands leads to Fermi surface nesting with the wave vector $\mathbf{q} \cong 0.3c^*$. The CDW instability due to this nesting is expected to cause the phase transition associated with the resistivity anomaly at low temperature. The characteristics of metallic behavior in the crystallographic ab plane are explained on the basis of the unnested 2D Fermi surfaces.

Introduction

Recently, Greenblatt *et al.*[1] prepared single crystals of KMo_4O_6 by electrolysis of a mixture of K_2MoO_4 and MoO_3. Their X-ray diffraction analysis shows that the structure of the compound is similar to that of $NaMo_4O_6$ prepared by Torardi and McCarley,[2] which contains chains of trans-edge-sharing Mo_6 octahedra. Also, the electrical resistivity and magnetic susceptibility measurements on crystal samples[1] show that KMo_4O_6 is metallic along the direction of the chains of Mo octahedra down to 100 K, below which it undergoes a metal-insulator phase transition, while KMo_4O_6 remains metallic along the direction perpendicular to these chains down to 2 K with no transition to semiconducting behavior. The conductivity of the latter case is found to be much lower than that of the former. This suggests that the electronic properties of KMo_4O_6 should be highly anisotropic.

In the present work, we have undertaken the electronic band structure calculations of KMo_4O_6 on the basis of the extended Hückel tight-binding (EHTB) method[3] and analyzed the nature of its partially filled bands to examine the anisotropy of the electronic conductivity described above and the problem of whether a resistivity anomaly at low temperature is associated with a charge density wave (CDW) instability. The atomic parameters used in our calculations are summarized in Table 1.

Crystal Structure

Previous to a discussion of the electronic band structure of KMo_4O_6, it is necessary to describe the essential features of its crystal structure. KMo_4O_6 is made up of two Mo_4O_4 chains of trans-edge-sharing Mo_6 octahedra per unit cell which are linked by trigonally bonded oxygen atoms. K^+ ions reside in approximately cubic coordination in the channels between the cross-linked chains. The structure of this compound is tetragonal (space group $P\bar{4}$).[1] A projection view of the resulting structure along the c axis is shown in Figure 1. The Mo_6O_{16} cluster in KMo_4O_6 is also shown in Figure 2, with the main interatomic distances collected in Table 2.

In an alternative description, the trans-edge-sharing Mo chains of this molybdate may be considered as constructed from two kinds of inoganic fragments, apical MoO_5 and basal MoO_4 (for the purpose of clarity, the Mo-O bonds of each fragment are represented by a thick line.) as shown in Figure

Table 1. Atomic Parameters Used in the EHTB Calculations: H_{ii} (eV) and ξ (Valence Orbital Ionization Potential and Exponent of the Slater-type Orbital)[a,b]

atom	orbital	H_{ii}	ξ_1 (c_1)	ξ_2 (c_2)
Mo	4d	−10.50	4.54(0.5899)	1.90(0.5899)
	5s	−8.34	1.96	
	5p	−5.24	1.90	
O	2s	−32.3	2.275	
	2p	−14.8	2.275	

[a]The d orbital of Mo is given as a linear combination of two Slater-type orbitals, and each exponent is followed by the weighted coefficient in parentheses. [b]A modified Wolfsberg-Helmholtz formula is used to calculate H_{ij}.[8]

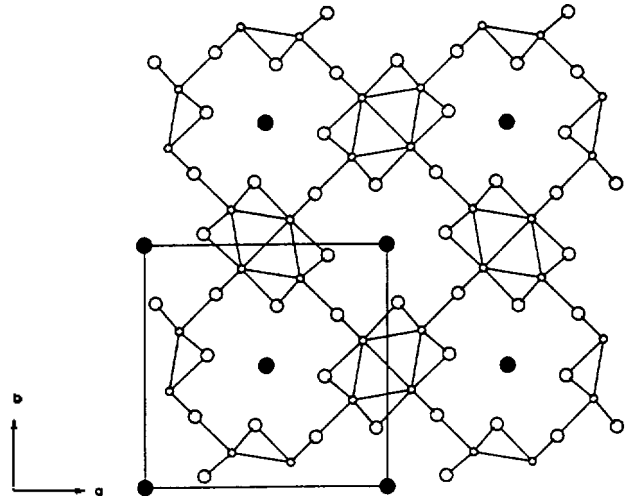

Figure 1. Projection of the tetragonal KMo_4O_6 structure viewed along the c axis. The small and large open circles represent Mo and O atoms, respectively. The K^+ ions are shown as darkened circles.

2. These fragments are seen as the remnants of an octahedron from which one or two ligands have been removed. This can provide an elementary scheme for simplifying the interpretation of rather complex electronic structure of this compound and thereby play a crucial role in determining the nature of the low-lying portion of the Mo *d*-block bands. A more detailed picture of bonding in this molybdenum oxide compound is discussed below.

Band Electronic Structure

Given the oxidation states of K^+ and O^{2-}, there are 3.25 electrons per molybdenum atom in the d-block bands of KMo_4O_6, so that the low-lying part of the *d*-block bands is filled. Figure 3 shows the dispersion relations of the three *d*-block bands near the Fermi level calculated for the $Mo_8O_{12}^{2-}$ lattice of KMo_4O_6 along several symmetry lines of the first Brillouin zone. With the two formula units per unit cell, we have 26 electrons to fill these bands. The dashed line refers to the Fermi level (e_f = −10.14 eV) corresponding to this

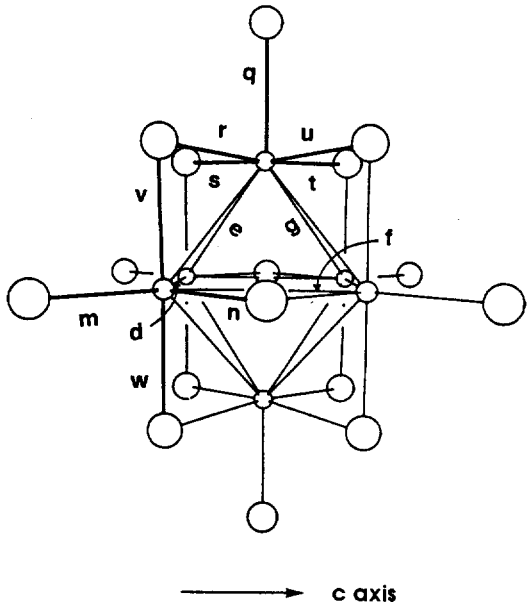

Figure 2. Mo_8O_{16} cluster unit having the same geometry as in the KMo_4O_6 solid. The labels *m*, *n*, and *q*-*w* indicate Mo-O distances, and *d*-*g* identify Mo-Mo distances.

Table 2. Bond Distances (Å) Calculated from Crystal Data in Ref. 1

bond		KMo_4O_6
Mo-Mo	d	2.75
	e	2.77
	f	2.88
	g	2.79
Mo-O	m	2.01
	n	2.04
	q	2.07
	r	2.04
	s	2.03
	t	2.05
	u	2.03
	v	2.06
	w	2.07

electron counting. Since the transport properties of a metal are primarily determined by the partially filled bands, we focus on the low-lying part of the *d*-block bands. The O 2s and 2p bands are lying lower than the Mo d bands shown in Figure 3. Each of the three d-block bands shown in Figure 3 consists of two subbands. Of these three, the bottom two bands *a* and *b* are cut by the Fermi level and the bottom of the other band *c* lies slightly above the Fermi level. The most important feature is the anisotropy in the band dispersion curves. The bands are nearly flat along the ΓX, XM, and ΓM lines; *i.e.*, the directions perpendicular to the edge-sharing chain, while the bands are strongly dispersive along the ΓZ line; *i.e.*, the chain direction corresponding to the crystallographic *c* axis. The large slopes of the bands across

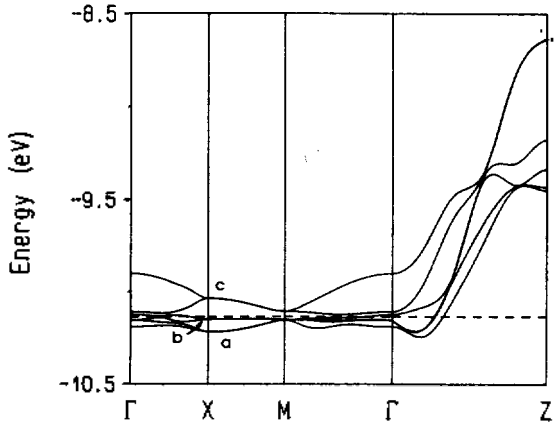

Figure 3. Dispersion relations of the three d-block bands near the Fermi level calculated for the $Mo_8O_{12}^{2-}$ slab of KMo_4O_6, where the dashed line represents the Fermi level. $\Gamma=(0, 0, 0)$, $X=(a^*/2, 0, 0)$, $M=(a^*/2, b^*/2, 0)$, and $Z=(0, 0, c^*/2)$.

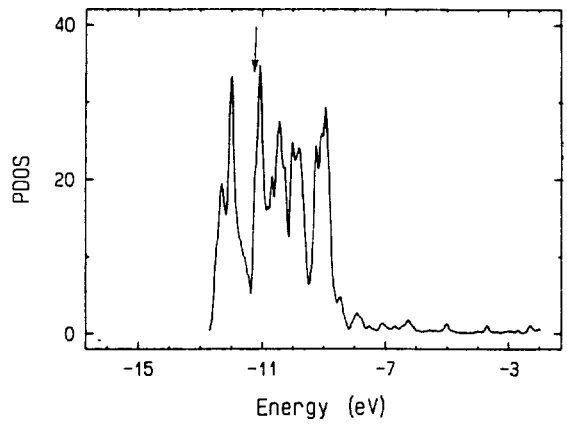

Figure 4. Projection of the density of states on the 4d orbitals calculated for the 3D Mo sublattice of KMo_4O_6. The Fermi level for the d electron count on the Mo sublattice chosen to preserve the formal oxidation state of Mo in KMo_4O_6 is represented by the arrow.

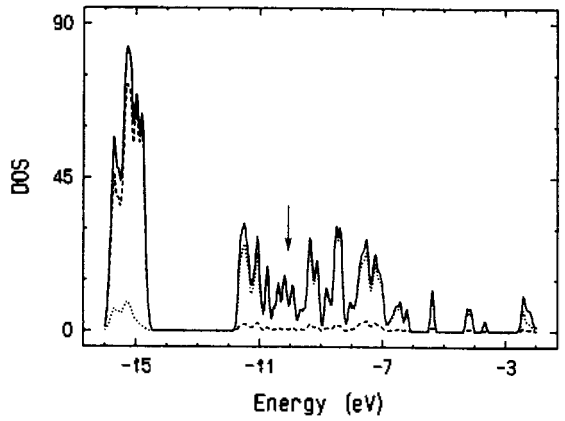

Figure 5. Plots of total DOS (solid line), Mo 4d contribution (dotted line) and O 2p contribution (dashed line) to the total DOS for the $Mo_8O_{12}^{2-}$ slab of KMo_4O_6. The Fermi level is indicated by the arrow.

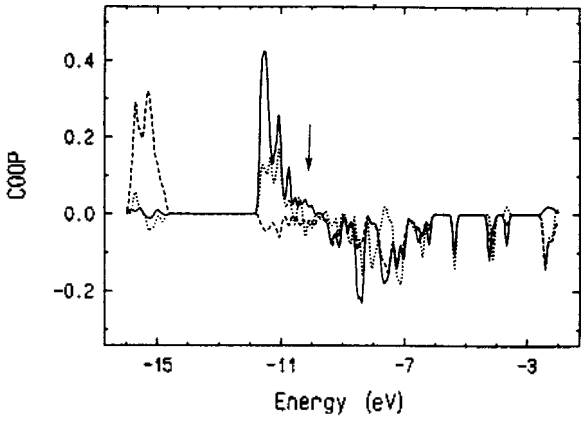

Figure 6. COOP curves for intracell Mo-Mo (solid line), intercell Mo-Mo (dotted line), and Mo-O bonds (dashed line) of the edge-sharing chains in KMo_4O_6. The Fermi level is indicated by the arrow.

the Fermi level are indicative of a small effective mass for the conduction electrons leading to a good electrical conductivity.[4] The conduction electrons present in the conduction band edge should be much more delocalized along the chain direction than perpendicular to this direction, and thus low-dimensional properties of this molybdenum oxide are strongly expected.

One (band *a*) of the two partially filled bands is crossing the Fermi level along c^* axis (*i.e.*, chain direction in real lattice space), but not along the other reciprocal axes. The other (band *b*) is crossing the Fermi level along the three orthogonal directions. Consequently, KMo_4O_6 possesses the partially filled bands of both one-dimensional (1D) and 3D character. In general, low-dimensional metals exhibit resistivity anomalies originating from the electronic instability such as a CDW state when their Fermi surfaces are nested.[5] The presence of the 1D band suggests that the CDW instability can occur in KMo_4O_6. However, even if KMo_4O_6 undergoes a CDW transition, it may still remain metallic due to the presence of the 3D band.

We expect that the main contribution to Mo-Mo bonding of the chain should arise from the low-lying portion of the d-block bands because only about the bottom one third of the bands will be filled for the formal d electron count of 3.25 per atom. Figure 4 represents the projected density of states (PDOS) on the 4d atomic orbitals for the Mo sublattice before interaction with the surrounding oxygens. The contribution of the Mo 4d orbitals spreads over 4 eV. Such a broadening reflects some significant metal-metal interactions. The DOS curves after interaction of the Mo sublattice with the oxide sublattice are shown in Figure 5. The DOS peak due to the Mo 4d orbitals is pushed up into antibonding states by the oxygen 2p. This results in a shift of the Fermi level up in energy by almost 1 eV as the d electron count on the Mo sublattice is chosen to preserve the formal oxidation state of Mo in KMo_4O_6. This clearly indicates that the bonding interactions between the two sublattices are not simply ionic, but significantly covalent. States between -16 and -14.5 eV are mainly oxygen 2p in composition.

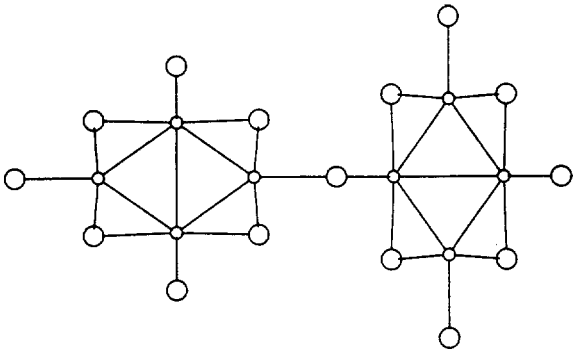

Figure 7. Structural models for the interchain interactions of the double edge-sharing chains having the same geometry as in the solid. The small and large open circles represent Mo and O atoms, respectively. The chain directions (*i.e.*, the crystallographic c directions) are perpendicular to the figure plane.

Let us now turn our attention to the problem for understanding the Mo-Mo and Mo-O bonding within the chains with the help of the crystal orbital overlap population (COOP) curves.[6] In order to confirm the essential validity of the above description, we examine the overlap populations of the crystal orbitals for the 3D molybdenum oxide solid. The overlap populations[7] between two atoms are correlated to the bond strength, and the higher the population, the stronger the bond. Consider first both intracell and intercell Mo-Mo bonds. As shown in Figure 6, most of the levels below e_f are Mo-Mo bonding. The total overlap populations at the Fermi level (for the formal d count of 3.25 per atom) give the values of 0.25 and 0.10 for intracell and intercell Mo-Mo bonds, respectively. These are obtained by integrating the COOP curves up to the Fermi level. The contributions of oxygen 2p bands to Mo-Mo overlap populations are negligible. The pairs of Mo atoms within the cell appear rather strongly bonded, compared with those between cells. The large positive COOP peak which lies in the region of the oxygen 2p bands is indicative of Mo-O bonding, as predicted.

Interchain Interactions

In the preceding we analyzed the metal-metal bonding in the edge-sharing Mo chains of KMo_4O_6. It is of interest to examine the orbital interactions between the chains coupled by the bridging three-coordinate oxygens to provide an electronic explanation for the electrical properties along the directions perpendicular to the chain. Figure 7 represents the double edge-sharing chains linked to each other through oxygen atoms, where the chain direction (crystallographic c axis) is perpendicular to the figure plane. We calculated the PDOS on 4d orbitals of a single chain and that of a double chain and compared them to that of the whole solid. For both chains, the PDOS curves (Figures 8 and 9) are very similar in shape and position to the PDOS curves on 4d of the 3D solid (Figure 5). In particular, the shape of the PDOS curves with a maximum at both band edges, which is indicative of the typical 1D DOS, is found again for the DOS of the 4d Mo bands of the 3D solid. These strong similarities of DOS curves indicate that the electronic states of the conduction bands in KMo_4O_6 are made up of the crystal orbitals of isolated single trans-edge-sharing Mo chain and the states are scarcely affected by the interaction between chains. In other words, this weak interchain interaction serves to reduce the delocalization of electrons in the bottom of the conduction bands of KMo_4O_6 along the interchain directions, and they should move as if they were in isolated single chain.

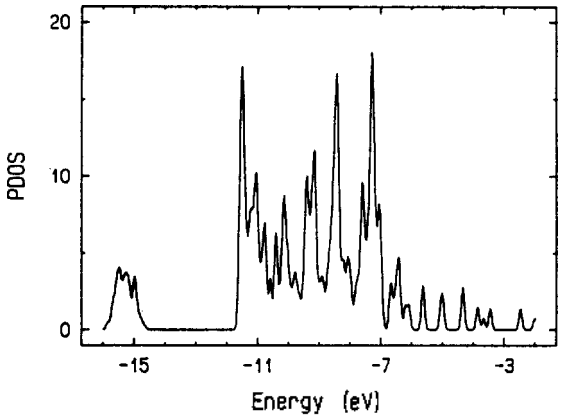

Figure 8. Plot of PDOS on 4d orbitals for the single chain of Figure 7.

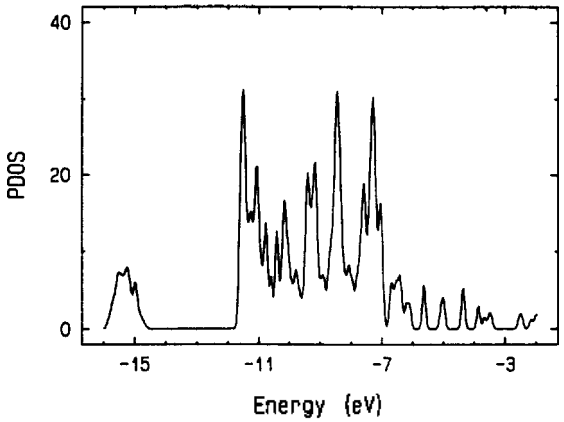

Figure 9. Plot of PDOS on 4d orbitals for the double chain of Figure 7.

Fermi Surfaces

The Fermi surfaces associated with the two partially filled bands a and b of Figure 3 are shown in parts a and b of Figure 10(a), respectively. In part a of Figure 10(a), the Fermi surfaces consist of one pair of the 1D warped lines. The slight warping of the Fermi surfaces reflects the fact that interactions along the interchain directions are very small but nonvanishing. The part b of Figure 10(a) essentially consists of the Fermi surfaces having a shape of overlapping circles when combined into one in the extended zone scheme. The cross section of these Fermi surfaces is closed in all directions. Furthermore, these Fermi surfaces are slightly elongated along the direction perpendicular to the c^* direction. Thus, the electrical conductivity of KMo_4O_6

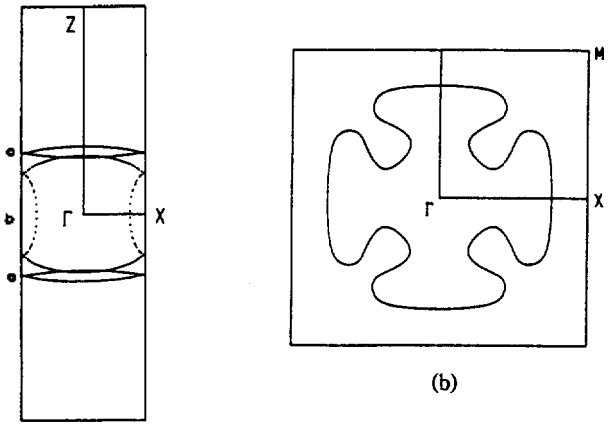

Figure 10. Cross sections of the Fermi surfaces in (a) the a^*c^* plane at the b^*-height of 0 and (b) the a^*b^* plane at the c^*-height of 0, associated with the two partially filled bands of Figure 3.

should be much higher along the c^* direction (*i.e.*, the chain direction) than along the directions perpendicular to it, since each surface has a much larger cross sectional area along the c^* direction. This is consistent with the observation that the room temperature electrical resistivity measured along the chain direction is approximately a factor of 3 lower than measured perpendicular to these chains.[1]

For the Fermi surfaces of the band a shown in Figure 10(a), the lower piece is nested to the upper one by a wave vector $\mathbf{q}\cong 0.3c^*$. A metallic system with a nesting vector $\mathbf{q}$ is susceptible to form a CDW state of wave vector $\mathbf{q}$. In case that the resistivity anomaly of KMo_4O_6 originates from the CDW instability associated with this Fermi surface nesting, the CDW instability would necessarily induce incommensurate superlattice modulations into the lattice along the c^* direction at low temperatures below ~100 K. The CDW formation would open a band gap at the Fermi level, so that it typically can induce a metal-insulator phase transition. However, the crystal structure of KMo_4O_6 reveals no evidence of diffuse spots indicative of incommensurate behavior at a temperature below its phase transition.[1] It is probable that the insulating state of KMo_4O_6 is a spin density wave and not a CDW or a new structural phase. Further experimental work is necessary to understand the nature of the insulating state of the compound.

Since the 2D Fermi surfaces shown in Figure 10(b) will not be affected by the nesting, they are not expected to give rise to a metal-insulator (MI) transition. This expectation is consistent with the observation[1] that KMo_4O_6 remains metallic down to 2 K in the crystallographic ab plane.

Concluding Remarks

Our calculations show that KMo_4O_6 has both 1D and 3D bands, and its electrical conductivity is much stronger along the chain of condensed molybdenum octahedra than in the plane perpendicular to it. A CDW transition due to an electronic instability associated with the Fermi surface nesting is likely to be responsible for the resistivity anomaly at low temperature. However, the phase transition associated with the resistivity anomaly may not be caused by the CDW instability because of the absence of an incommensurate superlattice modulation in the solid lattice. Further studies are necessary to resolve the difference between theory and experiment concerning its origin. The characteristics of metallic behavior in the crystallographic ab plane can be well accounted for by the occurrence of the unnested 2D Fermi surfaces which is most likely to be one of the factors impeding the electronic instability toward MI transition.

It is noted that KMo_4O_6 has an empty band whose bottom lies very close to the Fermi level. Therefore, it would be important to search for the presence of the CDW vectors and their temperature dependence to understand the nature of the phase transition in KMo_4O_6. A similar phenomenon has been observed for the molybdenum blue bronze $A_{0.3}MoO_3$ (A=K, Rb).[9]

References

1. Ramanujachary, K. V.; Greenblatt, M.; Jones, E. B.; McCarrol, W. H. *J. Solid State Chem.* **1993**, *102*, 69.
2. Torardi, C. C.; McCarley, R. E. *J. Am. Chem. Soc.* **1979**, *101*, 3963.
3. Whangbo, M.-H.; Hoffmann, R. *J. Am. Chem. Soc.* **1978**, *100*, 6093.
4. Cox, P. A. *The Electronic Structure and Chemistry of Solids*; Oxford University Press: Oxford, U. K., 1987.
5. Canadell, E.; Whangbo, M.-H. *Chem. Rev.* **1991**, *91*, 965.
6. Hoffmann, R. *Solids and Surfaces. A Chemist's View of Bonding in Extended Structures*; VCH Publishers: New York, 1988.
7. Mulliken, R. S. *J. Chem. Phys.* **1955**, *23*, 1833, 2343.
8. Ammeter, J. H.; Bürgi, H.-B.; Thibeault, J. C.; Hoffmann, R. *J. Am. Chem. Soc.* **1978**, *100*, 3686.
9. Whangbo, M.-H.; Schneemeyer, L. F. *Inorg. Chem.* **1986**, *25*, 2424.